Journal of Orthopaedic Translation 45 (2024) 197–210

Contents lists available at ScienceDirect

Journal of Orthopaedic Translation

journal homepage: www.journals.elsevier.com/journal-of-orthopaedic-translation

Original Article

Therapeutic potential of a prominent dihydroxyflavanone pinocembrin for osteolytic bone disease: *In vitro* and *in vivo* evidence

Guoju Hong [a,b], Shuqiang Li [c], Guanqiang Zheng [d], Xiaoxia Zheng [e], Qunzhang Zhan [e], Lin Zhou [f,**], Qiushi Wei [a,b,***], Wei He [a,b,****], Zhenqiu Chen [g,*]

[a] *Traumatology & Orthopaedics Institute, Guangzhou University of Chinese Medicine, Guangzhou, Guangdong, 510378, PR China*
[b] *Department of Orthopaedics, The Third Affiliated Hospital of Guangzhou University of Chinese Medicine, Guangzhou, Guangdong, 510378, PR China*
[c] *Department of Oncology, The Third Affiliated Hospital of Guangzhou University of Chinese Medicine, Guangzhou, Guangdong, 510378, PR China*
[d] *Department of Rehabilitation, The Third Affiliated Hospital of Guangzhou University of Chinese Medicine, Guangzhou, Guangdong, 510378, PR China*
[e] *The Third Clinical Medical College, Guangzhou University of Chinese Medicine, Guangzhou, Guangdong, 510405, PR China*
[f] *Department of Endocrinology, Key Laboratory of Biological Targeting Diagnosis, Therapy and Rehabilitation of Guangdong Higher Education Institutes, The Fifth Affiliated Hospital of Guangzhou Medical University, Guangzhou Medical University, Guangzhou, 510700, PR China*
[g] *Department of Orthopaedics, The First Affiliated Hospital of Guangzhou University of Chinese Medicine, Guangzhou, Guangdong, 510405, PR China*

ARTICLE INFO

Keywords:
Osteoclast
Osteolysis
Pinocembrin
RANKL
Reactive oxygen species

ABSTRACT

Background/objective: As the pivotal cellular mediators of bone resorption and pathological bone remodeling, osteoclasts have emerged as a prominent target for anti-resorptive interventions. Pinocembrin (PIN), a predominant flavonoid found in damiana, honey, fingerroot, and propolis, has been recognized for its potential therapeutic effects in osteolysis. The purpose of our project is to investigate the potential of PIN to prevent bone resorption in ovariectomized (OVX) mice by suppressing osteoclast production through its underlying mechanisms.

Methods: The study commenced by employing protein-ligand molecular docking to ascertain the specific interaction between PIN and nuclear factor-κB (NF-κB) ligand (RANKL). Subsequently, PIN was introduced to bone marrow macrophages (BMMs) under the stimulation of RANKL. The impact of PIN on osteoclastic activity was assessed through the utilization of a positive TRAcP staining kit and a hydroxyapatite resorption assay. Furthermore, the study investigated the generation of reactive oxygen species (ROS) in osteoclasts induced by RANKL using H_2DCFDA. To delve deeper into the underlying mechanisms, molecular cascades triggered by RANKL, including NF-κB, ROS, calcium oscillations, and NFATc1-mediated signaling pathways, were explored using Luciferase gene report, western blot analysis, and quantitative real-time polymerase chain reaction. Moreover, an estrogen-deficient osteoporosis murine model was established to evaluate the therapeutic effects of PIN *in vivo*.

Results: In this study, we elucidated the profound inhibitory effects of PIN on osteoclastogenesis and bone resorption, achieved through repression of NF-κB and NFATc1-mediated signaling pathways. Notably, PIN also exhibited potent anti-oxidative properties by mitigating RANKL-induced ROS generation and augmenting activities of ROS-scavenging enzymes, ultimately leading to a reduction in intracellular ROS levels. Moreover, PIN effectively abrogated the expression of osteoclast-specific marker genes (*Acp5*, *Cathepsin K*, *Atp6v0d2*, *Nfatc1*, *c-fos*, and *Mmp9*), further underscoring its inhibitory impact on osteoclast differentiation and function. Additionally, employing an *in vivo* mouse model, we demonstrated that PIN effectively prevented osteoclast-induced bone loss resultant from estrogen deficiency.

* Corresponding author. Department of Orthopaedics, The First Affiliated Hospital of Guangzhou University of Chinese Medicine, Guangzhou, Guangdong, 510405, PR China.
** Corresponding author. Department of Endocrinology, Key Laboratory of Biological Targeting Diagnosis, Therapy and Rehabilitation of Guangdong Higher Education Institutes, The Fifth Affiliated Hospital of Guangzhou Medical University, Guangzhou Medical University, Guangzhou, 510700, PR China.
*** Corresponding author. Traumatology & Orthopedics Institute, Guangzhou University of Chinese Medicine, Guangzhou, Guangdong, 510378, PR China.
**** Corresponding author. Traumatology & Orthopedics Institute, Guangzhou University of Chinese Medicine, Guangzhou, Guangdong, 510378, PR China.
E-mail addresses: gdsthgj@gmail.com (G. Hong), 912395010@qq.com (L. Zhou), weiqshi@126.com (Q. Wei), hewei1123@gzucm.edu.cn (W. He), chenzhenqiu2012@126.com (Z. Chen).

https://doi.org/10.1016/j.jot.2023.12.007
Received 29 September 2023; Received in revised form 27 December 2023; Accepted 30 December 2023
Available online 27 March 2024

Conclusion: Our findings highlight the potent inhibitory effects of PIN on osteoclastogenesis, bone resorption, and RANKL-induced signaling pathways, thereby establishing PIN as a promising therapeutic candidate for the prevention and management of osteolytic bone diseases.
The translational potential of this article: PIN serves as a promising therapeutic agent for the prevention and management of osteolytic bone diseases and holds promise for future clinical applications in addressing conditions characterized by excessive bone resorption. PIN is a natural compound found in various sources, including damiana, honey, fingerroot, and propolis. Its widespread availability and potential for therapeutic use make it an attractive candidate for further investigation and development as a clinical intervention.

1. Introduction

Being a dynamic and living tissue, bone undergoes an ongoing cycle of remodeling and regeneration, ensuring internal balance throughout an individual's life [1,2]. Disruption of bone stability and strength can significantly elevate the risk of fractures, leading to a considerable decline in quality of life and increased mortality associated with this condition [3]. Among various types of osteolytic bone diseases, postmenopausal osteoporosis is the most prevalent form, affecting approximately one-third of women aged fifty or older in the North America [4]. The intricate equilibrium between bone resorption driven by osteoclasts and bone formation initiated by osteoblasts plays a pivotal role in this mechanism [5]. Excessive osteoclast activity and increased numbers of osteoclasts are the primary contributors to the development of osteoporosis [6].

Osteoclasts are the unique multiple nuclear giant cells for bone resorption and are distinct from the lineage of hematopoietic precursor cells mononuclear macrophages [7]. The receptor activator of nuclear factor-κ B (NF-κ B) ligand (RANKL) is an important element for the differentiation and function of osteoclasts [8]. The binding of RANKL to RANK triggers the recruitment of bridging molecules known as TNF receptor-associated factors (TRAFs), notably TRAF6. This recruitment sets in motion a cascade of downstream signaling pathways, involving nuclear factor kappa-light-chain-enhancer of activated B cells (NF-κB), mitogen-activated protein kinases (MAPKs), such as p38, JNK, and ERK1/2. Subsequently, the activation of the transcription factor nuclear factor of activated T cells 1 (NFATc1) takes place. This orchestrated process initiates the differentiation of osteoclasts and the subsequent bone resorption. It accomplishes this by inducing the expression of specific genes associated with osteoclasts, including *Acp5*, *Cathepsin K*, *Atp6v0d2*, *Nfatc1*, *c-Fos*, and *Mmp9* [9].

Pinocembrin (PIN), a prominent dihydroxyflavanone abundantly found in propolis and various plants, has garnered significant interest due to its multifaceted therapeutic properties, encompassing anti-cardiac defect [10], anti-skin fibrosis [11], and anti-neuroinflammation [12]. PIN has been shown to directly impact osteoblast differentiation and mineralization [13]. Notably, recent research has elucidated that PIN can modulate the autophagy of osteocytes, counteracting the inhibitory effects of glucocorticoids on bone necrosis [14]. Given these intriguing findings, it would be worthwhile to investigate whether PIN also exerts anti-osteolytic effects on bone resorption by impeding osteoclast formation and functions, potentially positioning PIN as a promising therapeutic candidate for combating osteolysis.

Nonetheless, the cellular and molecular impacts of PIN on osteoclast development and function remain uncertain. In this investigation, we recognized PIN's potential to impede osteoclastogenesis, as inferred from initial compound screenings. Our objective was to assess how PIN influences the formation of osteoclasts induced by RANKL, as well as bone resorption, and to delve into the mechanisms underlying this influence. Our findings demonstrate that PIN possesses the capability to halt both osteoclast formation and the resorption activity of osteoclasts by diminishing the signaling pathway initiated by RANKL. These outcomes suggest that PIN could be a promising candidate for combating osteoclast-related bone loss, offering potential as a novel therapeutic agent.

2. Materials and methods

2.1. Materials and reagents

Alpha-modified eagle medium (α-MEM) and fetal bovine serum (FBS) were purchased from Gibco-BRL (Sigma–Aldrich, St. Louis, MO, USA). PIN was purchased from CSNpharm (Catalog No. CSN15662, Shanghai, P.C. China) and dissolved in dimethylsulfoxide (DMSO). Tartrate-resistant acid phosphatase (TRAcP) staining kit were purchased from Sigma–Aldrich (St. Louis, MO, USA). Macrophage colony-stimulating factor (M-CSF) was provided by R&D Systems (Minneapolis, MN, USA). Recombinant murine sRANK-ligand protein (rm-sRANKL) was obtained from PeproTech (Rocky Hill, NJ, USA).

2.2. PIN–RANKL molecular docking

PIN's 2D structures were downloaded from PubChem (CID: 68071, Fig. S1), whereas the 3D structures were converted, and the ligand was optimized using LigPrep from the Schrödinger Discovery Suite. Various possible ionization states were produced, and all of them were transferred to the subsequent docking stage. The optimized structure of RANKL-RANK was submitted to POCASA for potential binding site prediction. The initial and refined structures were contrasted with each other through Ramachandran Plot. The optimized model of RANKL was investigated with Sitemap to identify the binding sites. Subsequently, a receptor grid was generated to consider all feasible binding sites for the docking stage. In the docking procedure, we determined the docking position of PIN on RANKL using Glide XP docking and compared docking scores. The conformation with the highest docking score was chosen. Additionally, we utilized the Molecular Mechanics-Generalized Born Surface Area procedure to assess how PIN's binding affected protein stability and chemical bond formation.

2.3. In vitro assay of osteoclastogenesis

By flushing out the marrow from the femur and tibia obtained from 8-week-old C57BL/6J mice, we harvested bone marrow macrophages (BMMs) and assessed their morphology using light microscopy. An α-MEM solution containing M-CSF (50 ng/mL) was then used to culture the harvested cells. To facilitate adherence, we seeded 6×10^3 BMMs in each well of 96-well plates and incubated them in the complete α-MEM for 24 h. Following this, the cells were incubated for 5–7 days in an atmosphere containing 5 % CO_2 at 37 °C to promote osteoclast differentiation. We investigated the impact of PIN on osteoclast differentiation by adding rm-sRANKL (50 ng/mL) and M-CSF to the culture media every other day starting from Day 2, along with various concentrations of PIN. Once osteoclasts had formed, we conducted TRAcP staining by using the specific kit, and cells exhibiting three or more nuclei and positive for TRAcP ($TRAcP^+$) were identified as osteoclasts.

2.4. MTS assay for cytotoxicity

Cytotoxicity of PIN on BMMs was estimated by using the commercial MTS (3-(4,5-dimethylthiazol-2-yl)-5-(3-carboxymethoxyphenyl)-2-(4-sulfophenyl)-2H-tetrazolium) assay kit (Promega Corporation, Madison,

WI, USA). Briefly, BMMs were seeded into a 96-well plate (6×10^3 cells/well) and left overnight until being confluent. After that, the BMMs were stimulated in the presence or absence of different doses (0, 1, 5, 10, 20 to 50 μ M) of PIN for 48-h incubation. The concentration of MTS solution was 20 μ M. Cells was further incubated with MTS solution at 37 °*C* for 2 h. The absorbance at 490 nm of each well was evaluated using a microplate reader (BMG Labtech, Ortenberg, Germany).

2.5. Hydroxyapatite resorption assay

In order to detect function of mature osteoclast on bone resorption, BMM cells were cultured at a density of 1×10^5 cells/well onto a 6-well collagen-coated plates and stimulated to induce osteoclastogenesis by M-CSF (50 ng/mL) and rm-sRANKL (50 ng/mL) every two days until mature osteoclasts were produced. Then, RANKL-induced BMMs were then dissociated and detached gently from the original wells and equally harvested onto the wells of a 96-well hydroxyapatite-coated plate (Corning Inc., Corning, NY, USA). Different concentrations of PIN (2.5 and 5 μ M) were used to treat the cells for 48-h incubation. Half of the wells of each group were stained by TRAcP to show $TRAcP^+$ cells. In contrast, the left wells were bleached in order to clean the cells and expose the resorption area. Images of stained $TRAcP^+$ cells and resorption area were captured by a light microscopy and quantitatively analyzed.

2.6. Measurement of intracellular ROS production

Following a 60-min exposure to RANKL (50 ng/mL) and PIN (2.5 and 5 μ M), BMMs were subjected to incubation with Hank's balanced salt solution containing 5 mM H_2DCFDA in a light-free environment for 5 min. H_2DCFDA, a non-fluorescent probe, undergoes enzymatic oxidation and subsequent cleavage of the acetate groups, resulting in the generation of dichlorofluorescein (DCF), a highly fluorescent molecule. The fluorescence emitted by DCF was detected using an A1Si confocal microscope equipped with a NIKON 488 nm excitation light and 540 nm emission light. To determine the average fluorescence intensity, image analysis was performed using the ImageJ software.

2.7. Calcium (Ca^{2+}) oscillation measurement

BMMs were seeded with complete culture medium and incubated until reaching confluence. Subsequently, the cells were treated with or without the specified concentration of PIN for 1 h. As positive controls, cells were stimulated with rm-sRANKL and M-CSF in a same dose, while the negative control received M-CSF alone. After overnight incubation, cells from each group were washed twice with a washing buffer composed of Hanks' balanced salt solution containing 1 mM probenecid and 1 % FBS. Next, 100 μL per well of Fluo4 staining solution (Thermo Fisher Scientific, Waltham, MA, USA) was added to the cells and incubated at 37 °C, protected from light, for 45 min. Following the staining period, the cells were rinsed again with the washing buffer to remove excess staining solution and allowed to equilibrate at room temperature for 20 min. Using an inverted fluorescence microscope (Nikon, Tokyo, Japan), the fluorescence intensity excited at 488 nm was visualized. The captured images were subsequently analyzed using the corresponding Nikon software. Images were acquired at 2-s intervals for a duration of 1 min. Cells exhibiting at least two calcium peaks were identified as oscillating cells.

2.8. Luciferase reporter assays of NF-κ B and Nfatc1

The luciferase reporter assay was employed to assess the transcriptional activities of RANKL-induced NF-κB and NFATc1, as outlined in the following procedure. The RAW264.7 cell line (American Type Culture Collection, Manassas, VA, USA) was stably transfected with either p-NF-κB-TA-Luc or p-NAFTc1-TA-Luc luciferase reporter constructs, which are responsive to NF-κB and Nfatc1, respectively. The cells were then seeded onto a 48-well plate and allowed to incubate overnight at a density of 1.5×10^3 cells per well. On the subsequent day, the cells were pretreated with varying concentrations of PIN for 1 h, followed by an additional 6-h incubation for the Luc-NF-κB cells and a 24-h incubation for the Luc-NFATc1 cells, in the presence of rm-sRANKL stimulation (50 ng/mL). Finally, the cells were lysed, and luciferase activity was quantified using a luciferase reporter assay kit (Promega Corporation, Madison, WI, USA), along with a luminescence plate reader (BMG Labtech, Ortenberg, Germany).

2.9. Quantitative reverse-transcription polymerase chain reaction (qRT-PCR)

The mRNA levels of specific genes in osteoclasts were assessed using qRT-PCR. BMMs were cultured in 6-well plates with complete alpha-media supplemented with M-CSF (50 ng/mL) and rm-sRANKL (50 ng/mL) at a concentration of 1×10^5 cells. Simultaneously, varying concentrations of PIN were added for a duration of 5 days. When the positive control group exhibited osteoclast formation, total RNA was extracted using TRIZOL® reagent (Life Technologies, Carlsbad, CA, USA). Subsequently, reverse transcription was performed using a Reverse Transcription Assisted First Strand cDNA Synthesis Kit. qRT-PCR was conducted using SYBR Green PCR Master Mix, and the expression levels were normalized using *Gapdh* as a reference gene. The Comparative Ct (ΔCt) method was employed for data analysis. The primer sequences utilized for gene amplification are provided in **Table S1**.

2.10. Western blotting

BMMs were seeded at a density of 1×10^5 cells/well into six-well plates and incubated in the present or absend of PIN for 4 h ahead of the addition of rm-sRANKL (50 ng/mL) stimulation for the indicated times. The assessment of GTP-Rac1 involved culturing the cell lysis solution with PAK1 PBD protein (Sigma–Aldrich, St. Louis, MO, USA) and quantifying it using the active Rac1 PullDown and Detection Kit (Cell Signaling Technology, Danvers, MA, USA). Cells were lysed with radioimmune precipitation assay (RIPA) lysis buffer (Millipore, Burlington, MA, USA) plus protease and phosphatase inhibitor cocktail. In the GTP-Rac1 evaluation, cell lysis solution was cultured with PAK1 PBD protein (Sigma–Aldrich, St. Louis, MO, USA) and measured by an active Rac1 Pull-Down and Detection Kit (Cell Signaling Technology, Danvers, MA, USA). The cell samples were and centrifuged at 14,000 rpm for 30 min and the concentrations of the proteins were estimated by Bradford methods according to the manufacturer's kit (Bio-rad, Hercules, CA, USA). Equal amount of protein was separated by 10 % sodium dodecyl sulfate (SDS)-polyacrylamide gel and transferred onto polyvinylidene fluoride membrane (GE healthcare, Chicago, IL, USA). Afterward, the membranes were blocked in 5 % non-fat milk diluted in 1 × TBS-T buffer at room temperature for 1 h. Then membranes were firstly incubated with the primary antibodies overnight at 4 °*C*, followed by incubation with the specific secondary antibodies. Last, an Image-quant LAS 4000 (GE Healthcare, Chicago, IL, USA) was used to visualize blots of membrane bands. Detailed information regarding the antibodies used is listed in **Table S2**.

2.11. Ovariectomy (OVX)-induced osteolytic murine model

The animal experimentation was performed in compliance with the guidelines approved by the Institutional Animal Ethics Committee. Specifically, a cohort of 30 female C57BL/6J mice (11-week-old for sexually mature) was housed in individually ventilated cages under strictly controlled pathogen-free conditions. The mice were allocated randomly into three groups: the sham-operated group, the OVX group, and the OVX + PIN group, each consisting of 10 mice. After a period of

one-week acclimatization, the mice underwent either bilateral ovariectomy in the case of the OVX group and OVX + PIN group, or a sham procedure in the case of the sham-operated group.

Subsequently, the mice in the OVX + PIN group were intraperitoneally administered PIN at a dosage of 20 mg/kg, dissolved in DMSO, every day for a duration of six weeks. The optimal dosage of PIN had been determined prior to formal experimentation. In parallel, both the sham-operated group and the OVX group were administered an equivalent volume of a vehicle solution containing 1 % DMSO in phosphate-buffered saline (PBS) over the same treatment duration. All injections were administered using a strict aseptic technique. Regular health checks were conducted to promptly identify and address any complications. Ultimately, at the conclusion of the study, all mice were humanely euthanized. Subsequently, half of the mice from each group were subjected to *in vivo* biosafety assessment of PIN. The abdominal midline was surgically exposed, and blood was extracted from the abdominal aortas using a syringe. The collected blood samples were subjected to centrifugation to obtain serum, and the serum expression of TRAcP and C-terminal telopeptide (CTX-1) were quantified utilizing enzyme-linked immunosorbent assay (ELISA) kits sourced from R&D Systems (Minneapolis, MN, USA). Moreover, the left femurs were harvested for three-point bending test and micro-computed tomography (Micro-CT) scanning, while the right femurs were utilized for histomorphological analysis.

Concurrently, the second half of the mouse group had their organ specimens collected to evaluate potential hepatotoxicity, splenotoxicity, lung toxicity, cardiac toxicity, and renal toxicity by assessing organ dimensions and surface appearance. Additionally, blood samples were collected from the aortas of the mice for comprehensive blood count analysis using the BC6800 automated analyzer from Mindray (Shenzhen, China) in our clinical laboratory.

2.12. Three-point bending test

The three-point bending test was conducted to evaluate the biomechanical properties of the femurs extracted from the experimental mice. The femurs were dissected and subjected to a three-point bending test using a INSTRON 5566 UTM biomechanical tester (Instron® Product, Norwood, MA, USA). The femurs were placed horizontally on two supports and a load was applied vertically at the mid-diaphysis at a constant displacement rate of 0.5 mm/min until fracture occurred. The load and displacement were recorded, and the following biomechanical parameters were calculated: Yield point (N)/Body weight and Ultimate Point/Body weight. These parameters provide insights into the bone strength and resilience in the context of osteolytic conditions.

2.13. Micro-CT scanning

A high-resolution microCT (Skyscan 1176; Bruker, Belgium) was utilized to analyze fixed femurs. The scanning settings were as follows: X-ray source voltage at 60 kVp, current at 500 μA, and power at 40W. Pixel size was 9 μmol/L, and resolution was 20 μm. After reconstructing 2D and 3D images, a square region of interest (ROI) located 0.5 mm from the femoral growth plate was selected for qualitative and quantitative analysis. We employed the CT analyzer program (Bruker microCT, Kontich, Belgium) to measure parameters like bone volume/total volume (BV/TV), trabecular thickness (Tb.Th), trabecular number (Tb.N), and trabecular separation (Tb.Sep).

2.14. Bone histomorphometric analysis

Histomorphometric analysis of bone was employed to assess the trabecular bone quantity and osteoclast population within the femoral epiphysis. To initiate the analysis, the femur specimens were subjected to a two-week fixation period, followed by decalcification. Subsequently, microtome sections measuring 5 μm in thickness were meticulously prepared and subjected to staining procedures using hematoxylin-eosin (H&E) and TRAcP, facilitating the visualization of osteoclasts. Manual evaluation was then conducted to quantify the pertinent parameters, specifically the ratio of osteoclast surface area to bone surface area (Oc.S/BS) and the ratio of osteoclast number to bone surface area (N.Oc/BS).

2.15. Statistical analysis

The data in this study are represented as the mean ± standard deviation (SD), with a minimum of three independent replicate measurements. Statistical analysis involved employing the Student's t-test to compare means across various groups. A significance level of $P < 0.05$ was used to determine statistical significance, corresponding to a 95 % confidence interval.

3. Result

3.1. Identification of affinity of PIN-RANKL complex

To identify potential new combinations of PIN and RANKL, we developed a stepwise program to investigate the binding affinity between PIN and RANKL. A crystallographic structure of the RANK-RANKL complex was created as the fundamental model for fitting PIN-RANKL interactions (Fig. 1A). Based on the structural transformation of RANKL upon RANKL binding, we projected possible binding locations for PIN in hydrophobic waters involving hydrogen-bonded acceptors and donors (Fig. 1B–C). To be specific, the binding locus for PIN docking begins at residue SER229 on RANKL, crosses the binding groove between GLY228 and TRP263, and eventually extends down to HIS270 (Fig. 1D–E). Computational docking indicated a high affinity of RANKL for PIN (PIN binding free energy = −8.03 kcal/mol). Collectively, a high affinity between PIN and RANKL is suggested by our results by their complex non-covalent interactions (Fig. 1).

3.2. PIN inhibits RANKL-induced osteoclastogenesis in vitro

To examine how PIN influences the formation of osteoclasts induced by RANKL, we first evaluated the effect of PIN with varying concentrations on BMMs cell by osteoclastogenesis assays. Treatment with PIN resulted in suppressive effect on osteoclast formation in a dose-dependent manner (Fig. 2A–B). Furthermore, in a time-course analysis of osteoclastogenesis, cells were exposed to PIN (5 μM) at different time phases. It was shown that treatment of PIN resulted in an inhibitory effect of osteoclast differentiation from Day 3 to Day 6 rather than the early stage (Fig. 2C–D). To examine whether cellular toxicity might be related with the effect of PIN on inhabitation of osteoclast formation, an MTS assay was conducted to assess the cytotoxicity of PIN on the cells. The data revealed that no significant cytotoxicity of PIN was detected at the concentration of 20 μM or lower (Fig. 2E).

3.3. PIN suppresses osteoclasts functions in vitro

To further assess the impact of the PIN treatment on the bone resorption capacity of osteoclasts, we employed BMMs that were induced with RANKL to facilitate their differentiation into mature osteoclasts. They were then transferred to the hydroxyapatite resorption assay for a minimum duration of three days. Subsequently, the cells were subjected to PIN treatment and allowed to resorb for a period of 48 h. As depicted in Fig. 2F–G, our findings indicate that there were no significant differences observed in the number of osteoclasts among the different experimental groups. Nevertheless, upon close examination of the wells, it was evident that resorption pits were present, and notably, the extent of bone resorption area exhibited a noticeable reduction with escalating concentrations of PIN.

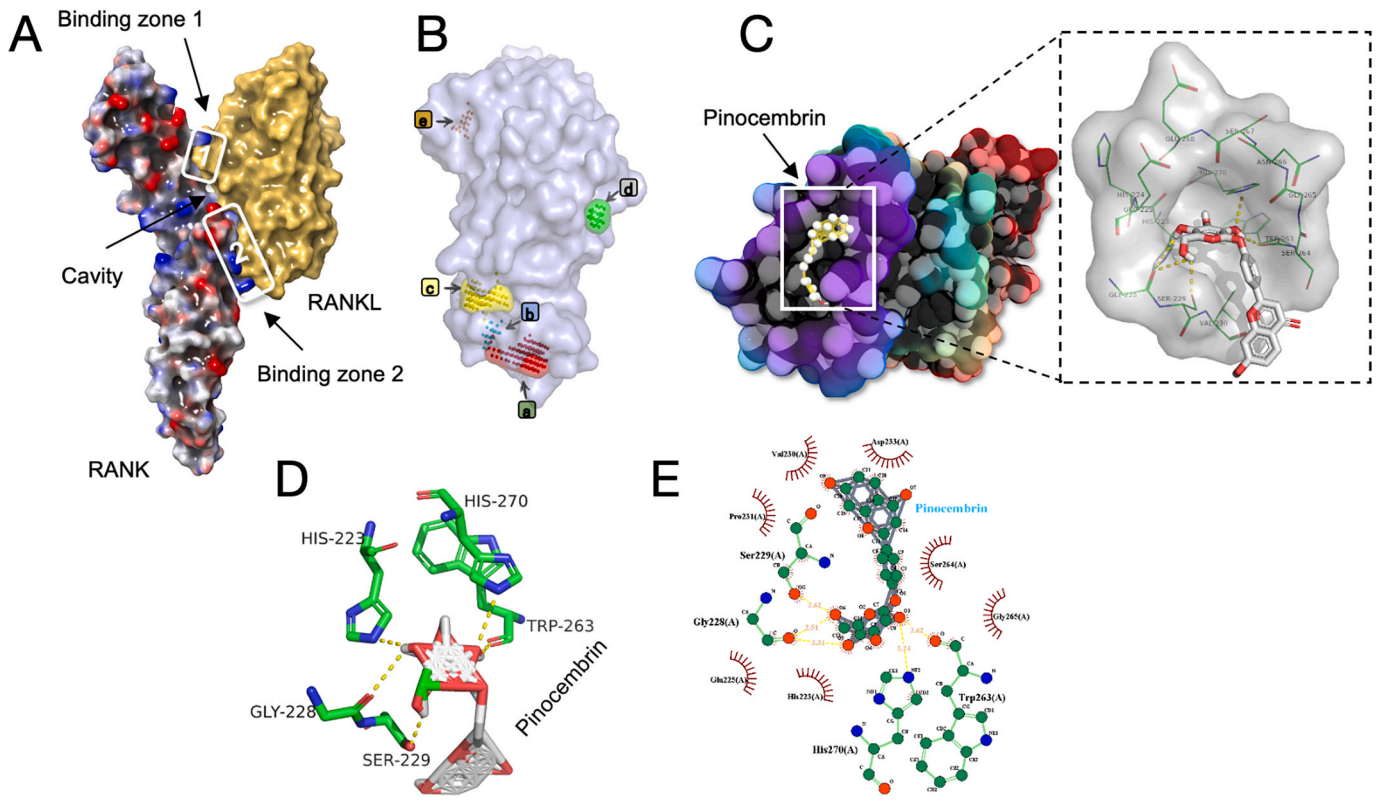

Fig. 1. The computational docking study of the PIN-RANKL interaction. (A) A 3D structural representation reveals that the interface of the RANK/RANKL complex. **(B)** The images presented depict all potential binding sites of RANKL. **(C)** Shown in the structural images are the docking pose and interactions between RANKL and PIN. The amino acid residues involved in bonding are highlighted in green color. **(D)** The 3D structural image illustrates the binding between PIN and RANKL. The amino acid residues contributing to the binding are depicted in green, while the yellow lines represent hydrogen bonds formed with polar atoms. **(E)** The 2D structural image presents the interactions between RANKL and PIN.

3.4. PIN suppresses ROS levels by inhibiting TRAF6/Rac1/NOX1 signaling pathway

We assessed the potential impact of PIN on the formation of ROS induced by RANKL using a cell-permeable fluorescent probe, H_2DCFDA. In comparison to the control group, the expression of intracellular ROS was significantly upregulated in the RANKL-treated group. Conversely, fluorescence intensity of DCF, indicative of ROS presence, was attenuated in each positively stained cell following treatment with PIN (Fig. 3A–B).

To elucidate the regulatory mechanism through which PIN modulates ROS levels, we examined the activation status of NADPH oxidase 1 (NOX1), the principal component responsible for ROS production. Our findings revealed that RANKL stimulation significantly increased the expression of NOX1, while administration of PIN (1, 2.5, 5 μM) suppressed this elevation (Fig. 3C–D). Considering that the activation of NOX1 requires the involvement of tumor necrosis factor receptor-associated factor 6 (TRAF6) and guanosine triphosphate (GTP)-bound Rac1 (GTP-Rac1), we delved deeper into the inquiry of whether PIN could hinder NOX1 activity by regulating the levels of TRAF6 and GTP-Rac1. RANKL treatment enhanced TRAF6 expression, whereas PIN administration (1, 2.5, 5 μM) reduced its expression (Fig. 3C–D). GTP-Rac1 serves as an intracellular component that plays a role in the activation of NOX1, exhibited an initial increase in activation following 5 min of stimulation with rm-sRANKL, but this activation showed a modest decrease after 15 min. Importantly, PIN administration (2.5 and 5 μM) dose-dependently suppressed this activation (Fig. 3E–F).

3.5. PIN increases the activity of antioxidant enzymes

To determine if PIN could reduce ROS levels by increasing the activity of antioxidant enzymes, we examined the expression levels of various enzymes, including heme oxygenase-1 (HO-1), catalase (CAT), and glutathione disulfide reductase (GSR). Our results demonstrated that when exposed to RANKL stimulation, there was a partial reduction in the expression of these enzymes, whereas their expression was restored in osteoclasts following administration of PIN (Fig. 3G–H). Collectively, our results demonstrate that PIN exhibits a dual mechanism in reducing intracellular ROS levels induced by RANKL: inhibiting ROS generation and enhancing ROS scavenging through the upregulation of antioxidant enzymes.

3.6. PIN restrains RANKL-induced calcium oscillations

RANKL can trigger Ca^{2+} oscillations that play a crucial role in stabilizing NFATc1 and facilitating its translocation into the nucleus. To assess the impact of PIN on RANKL-induced Ca^{2+}, we examined Ca^{2+} fluctuations in RANKL-treated BMMs using PIN. Three representative calcium flux patterns were recorded. It was observed that Ca^{2+} oscillations were evident in BMM cells treated with RANKL, whereas there were significantly fewer Ca^{2+} fluxes observed in PIN + RANKL-treated BMMs (Fig. 4A). Quantitative analysis revealed that PIN the magnitude of calcium ion fluxes induced by RANKL (Fig. 4B).

3.7. In vitro PIN suppressed osteoclast marker genes in the context of RANKL stimulation

Osteoclast differentiation is accompanied by the upregulation of

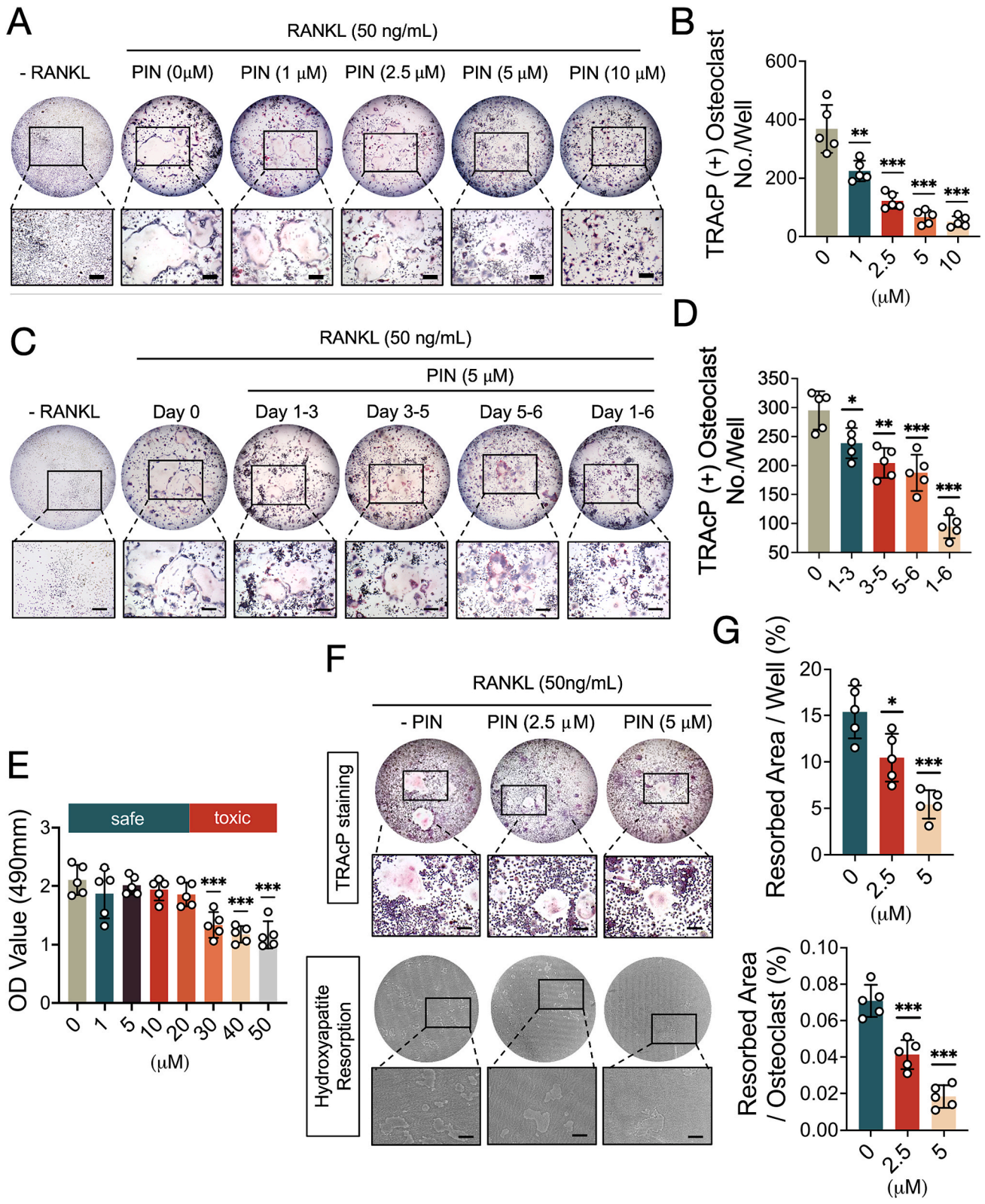

Fig. 2. Inhibition of RANKL-induced osteoclastogenesis and bone resorption by PIN without compromising cell survival. (A) BMM cells were cultured with M-CSF and rm-sRANKL in the presence of various concentrations of PIN for 5 days. Osteoclast formation was visualized by TRAcP staining. Representative images demonstrate a dose-dependent effect of PIN on RANKL-induced osteoclast differentiation. Scale bar = 100 μm. **(B)** Quantification of the number of TRAcP-positive multinuclear cells (containing three or more nuclei) following treatment with PIN (n = 5). **(C)** Exemplary illustrations depicting BMMs subjected to PIN treatment for the designated durations, as assessed through TRAcP staining. Scale bar: 100 μm. **(D)** A quantitative assessment of multinucleated osteoclast-like cells and exposed to PIN for the indicated timeframes (n = 5). **(E)** BMMs were exposed to different concentrations of PIN for 48 h, and cell viability was assessed using the MTS assay. **(F)** Representative images illustrate the quantification of hydroxyapatite resorption areas in relation to the number of TRAcP-stained osteoclasts. Scale bar: 100 μm. **(G)** Quantitative analysis of TRAcP-positive multinucleated cells and the percentage of hydroxyapatite surface area resorbed per osteoclast upon PIN treatment (n = 5). Statistical significance was evaluated by comparing it with the RANKL-treated group. (*$P < 0.05$, **$P < 0.01$, ***$P < 0.001$, versus RANKL-treated control).

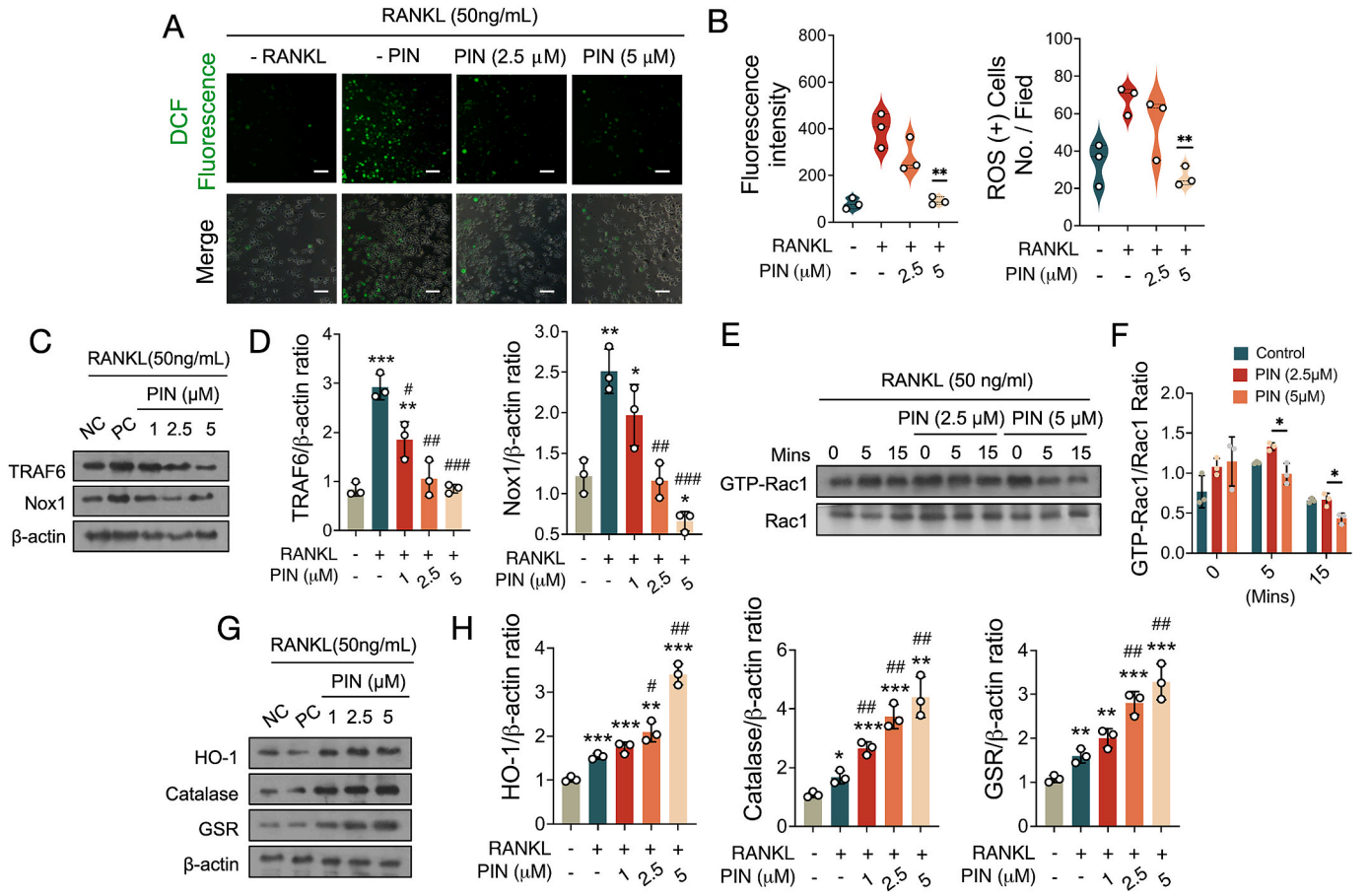

Fig. 3. PIN diminishes ROS levels in RANKL-induced osteoclasts via ROS siganling pathway. (A) Depicted are representative visualizations of RANKL-triggered intracellular ROS generation within BMMs, as discerned through the utilization of the cell-permeable oxidation-sensitive dye H_2DCFHDA. The upper panel illustrates the fluorescent DCF production (emitting a green color), while the lower panel exhibits merged images of DCF fluorescence and differential interference contrast for each group. Scale bar: 100 μm. **(B)** A comprehensive quantitative analysis of the DCF fluorescence intensity per osteoclast is presented (n = 3). Additionally, a quantitative appraisal of the number of ROS-stained cells in each field is provided (n = 3). (**P value < 0.01, versus RANKL-treated control) **(C)** Illustrated are representative images displaying the expression of TRAF6 and NOX1 in RANKL-treated osteoclasts following the addition of PIN. Protein expression levels have been normalized to β-actin. **(D)** A quantitative assessment of TRAF6 and NOX1, normalized to β-actin, is provided (n = 3). **(E)** Depicted are representative images exhibiting GTP-Rac1 expression at different time points (0, 5, and 15 min) after treatment with PIN. The cells were cultured with PAK1-PBD fusion protein, and protein expression levels are normalized to Rac1 levels. **(F)** A quantitative analysis of GTP-Rac1, normalized to Rac1, is presented (n = 3). **(G)** Shown are representative images of HO-1, CAT, and GSR protein expression. **(H)** A quantitative analysis of the protein band signal intensity of HO-1, CAT, and GSR, normalized to β-actin, is provided (n = 3). (*P value < 0.05, **P value < 0.01, ***P value < 0.001, versus blank control. #P value < 0.05, ##P value < 0.01, ###P value < 0.001, versus RANKL-treated control).

specific marker genes in response to RANKL signaling. In order to further elucidate the inhibitory effects of PIN on osteoclast differentiation, we assessed the mRNA expression levels of key osteoclast marker genes, including *Acp5*, *Cathepsin K, Atp6v0d2*, *Nfact1*, *c-fos*, and *Mmp9*. Through qRT-PCR analysis, we observed that the stimulation with RANKL increased the expression of these osteoclast-related genes, while the addition of PIN markedly reduced their expression. These findings clearly demonstrate that PIN exerts a potent inhibitory influence on the levels of osteoclast marker expression in an in *vitro* context (Fig. 4C).

3.8. PIN inhibits RANKL-induced NF-κB and MAPK signaling pathways

To gain further insights into the mechanism by which PIN suppresses RANKL-induced osteoclastogenesis, we investigated the involvement of NF-κB and MAPK signaling pathways. Luciferase assay results indicated that PIN primarily inhibited NF-κB activation at concentrations of 1, 2.5 and 5 μM (Fig. 5A). To explore the transient inhibitory effect of PIN on NF-κB, we examined the expression of IκB-α at different time points following RANKL treatment. As shown in Fig. 5B–C, PIN exhibited a statistically significant suppressive effect on IκB-α protein degradation at 20 min after RANKL stimulation.

To investigate the impact of PIN on MAPK signaling pathways, we examined the phosphorylation levels of Jnk, Erk, and p38 in the presence or absence of PIN administration at various time points (0, 10, 20, 30, and 60 min). Consistently, phosphorylation of Jnk, Erk, and p38 was inhibited compared to the control group (Fig. 5D). Specifically, as illustrated in Fig. 5E, PIN predominantly suppressed Erk phosphorylation from 10 to 60 min, with the most pronounced suppression observed late at 30–60 min after PIN treatment. The inhibition of Jnk and p38 phosphorylation by PIN is also demonstrated in Fig. 5E. These results indicate that PIN treatment can impact MAPK signaling pathways.

Collectively, the data clearly demonstrate that PIN suppresses NF-κB activity and inhibits MAPK phosphorylation in response to RANKL activation, subsequently exerting adverse effects on osteoclast formation and function.

3.9. Inhibition of Nfatc1 activity and downstream protein expression by PIN

To provide a comprehensive and intricate profile of the impact of PIN on osteoclast differentiation and function, we employed luciferase reporter gene profiling and Western blotting as analytical tools. These

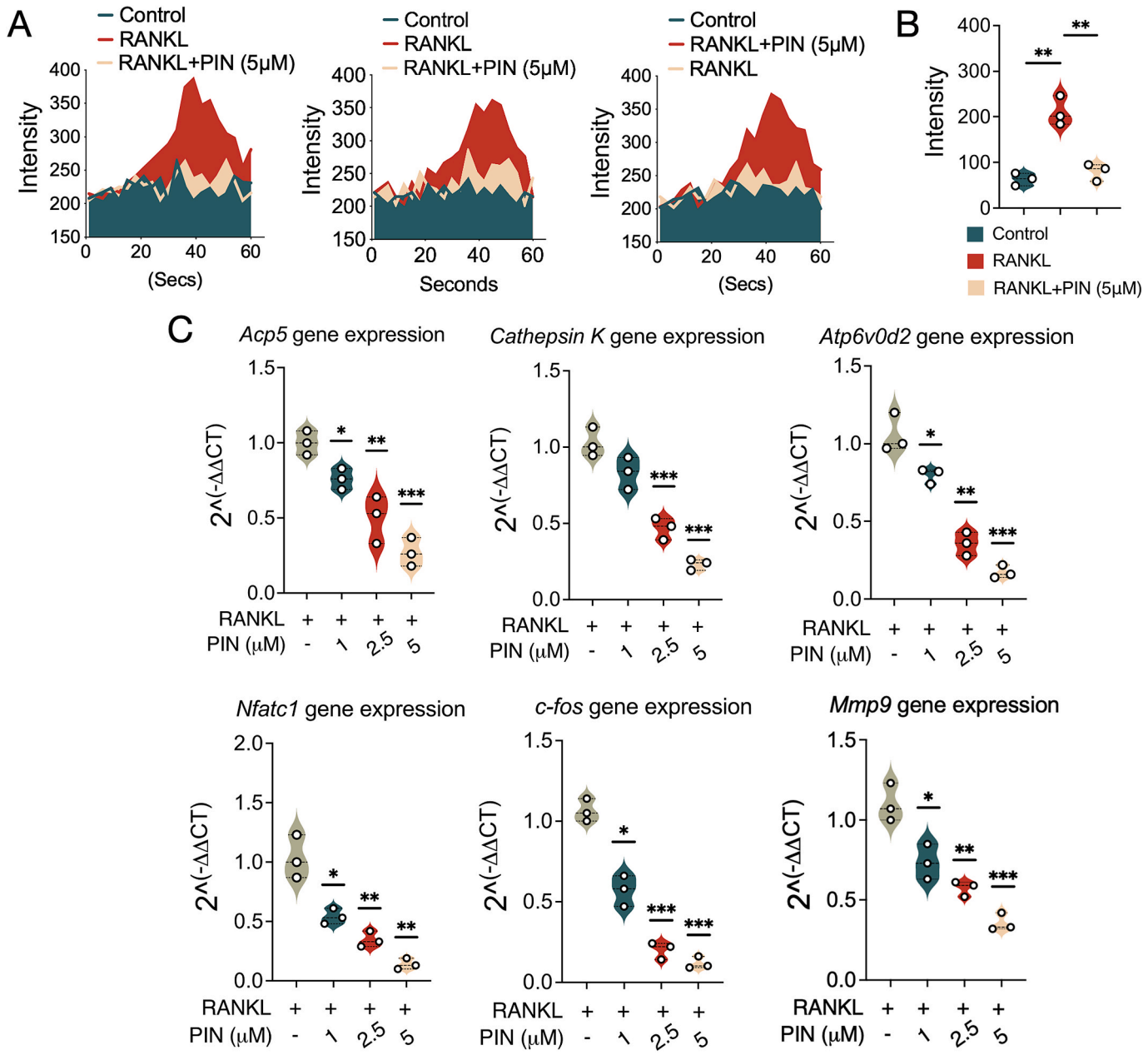

Fig. 4. PIN abolishes RANKL-induced calcium oscillation and osteoclast-related genes. (A) Calcium fluctuations were recorded in different experimental groups: the RANKL-treated group, the group treated solely with M-CSF (sham group), and the group stimulated with RANKL and PIN (5 μM). **(B)** The average intensity level per cell within each well was quantified. Calcium fluctuations were analyzed based on the condition of the cells, and the difference between the maximum peak intensity and the baseline intensity was measured. **(C)** The expression levels of the following genes were measured and normalized to *Gapdh*: *Acp5, Cathepsin K, Atp6v0d2*, *Nfatc1, c-Fos,* and *Mmp9*. (*$P < 0.05$, **$P < 0.01$, ***$P < 0.001$, versus RANKL-treated control).

techniques allowed for the measurement of Nfatc1 activity and downstream protein expression. Strikingly, PIN exhibited a significant dose-dependent reduction in Nfatc1 nuclei translocation, particularly at concentrations of 1, 2.5 and 5 μM, as demonstrated in Fig. 6A. Moreover, PIN exerted a remarkable inhibitory effect on the expression of Nfatc1 protein, which displayed substantial upregulation following 3 days of exposure to RANKL (Fig. 6B). Notably, the expression levels of downstream factors crucial for osteoclastic bone-resorbing activity, including V-ATPase-d2 and c-fos, were markedly attenuated following 3–5 days of PIN administration, whereas there were no changes for the Integrin α V expression (Fig. 6C). These findings collectively underscore the robust inhibitory effects of PIN on the expression of key genes and proteins, as well as the activity of essential transcriptional modulaters (such as Nfatc1) that play pivotal roles in osteoclastogenesis.

3.10. PIN alleviates progressive bone loss induced by estrogen deficiency

In our study, the *in vivo* experiments were designed to complement our *in vitro* findings by assessing the real-world therapeutic potential of PIN in a physiological context. Specifically, the animal trial aimed to investigate the effects of PIN on preventing bone loss in an estrogen-deficient osteolytic model. The experimental model involved OVX mice, which serve as a robust paradigm for studying bone loss in osteoporosis, along with sham-operated mice. Intraperitoneal administration of PIN or PBS was administered every other day for a span of 6 weeks (Fig. 7). Importantly, no severe adverse events or mortalities were observed throughout the OVX procedure or the intraperitoneal injection of PIN. Furthermore, PIN did not elicit any discernible effects on mouse body weight (Fig. S3), laboratory biochemistry (**Table S3**), or hematological profiles (**Table S4**). Meticulous

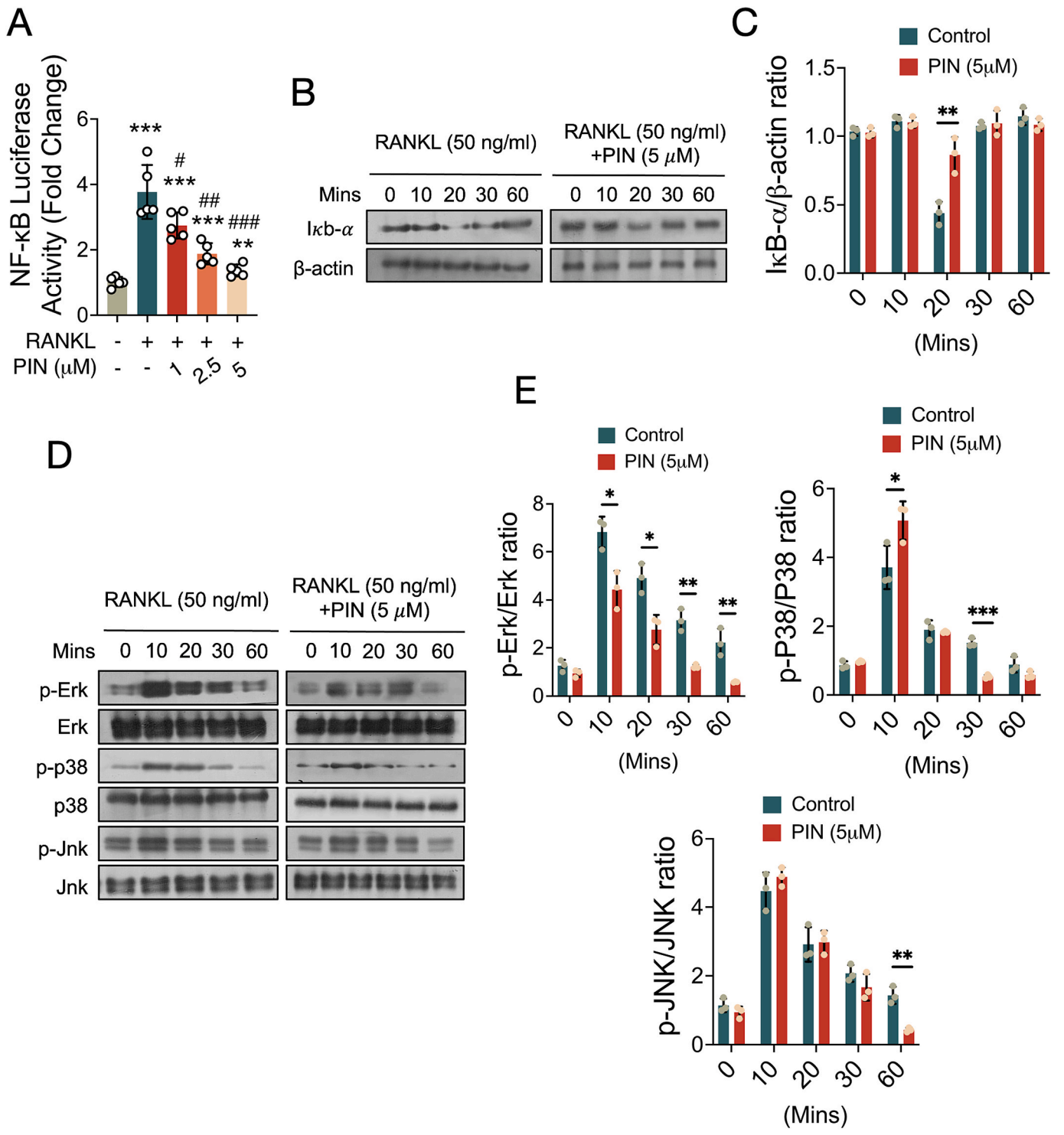

Fig. 5. PIN abolishes NF-κB activity and modulates the expression of IκB-α and MAPK signaling pathway. (A) Luciferase gene activity was assessed in RAW264.7 cells transfected with NF-κB luciferase construct and stimulated with rm-sRANKL (50 ng/mL) in addition to various concentrations of PIN. (**$P < 0.01$, ***$P < 0.001$, versus blank control. #$P < 0.05$, ##$P < 0.01$, ###$P < 0.001$, versus RANKL-treated control). **(B)** Protein lysates obtained from BMMs-induced osteoclasts pretreated with PIN (5 μM) and subsequently exposed to rm-sRANKL (50 ng/mL). Western blot analysis was conducted using specific antibodies against IκB-α and β-actin. **(C)** The relative results were quantified by determining the ratio of IκB-α to β-actin using Image J. **(D)** Representative images of western blot assay with antibodies against p-Erk, Erk, p-p38, p38, p-Jnk and Jnk. **(E)** The relative results were quantified by determining the ratio of p-Erk to Erk, p-p38 to p38, p-Jnk to Jnk. (*$P < 0.05$, **$P < 0.01$, ***$P < 0.01$ compared to RANKL-treated and PIN-untreated controls).

examination of vital organs, including the lung, liver, kidney, heart, and spleen, unveiled no notable alterations in size or surface characteristics across the treatment groups (Fig. S4).

Comparative analysis with the sham-operated group revealed a striking observation: PIN administration led to a substantial reduction in serum levels of TRAcP and CTX-1 in the OVX animal model, thus signifying its potent capacity to curtail bone resorption (Fig. 8A). Subsequently, the mice were humanely sacrificed, and their femurs were

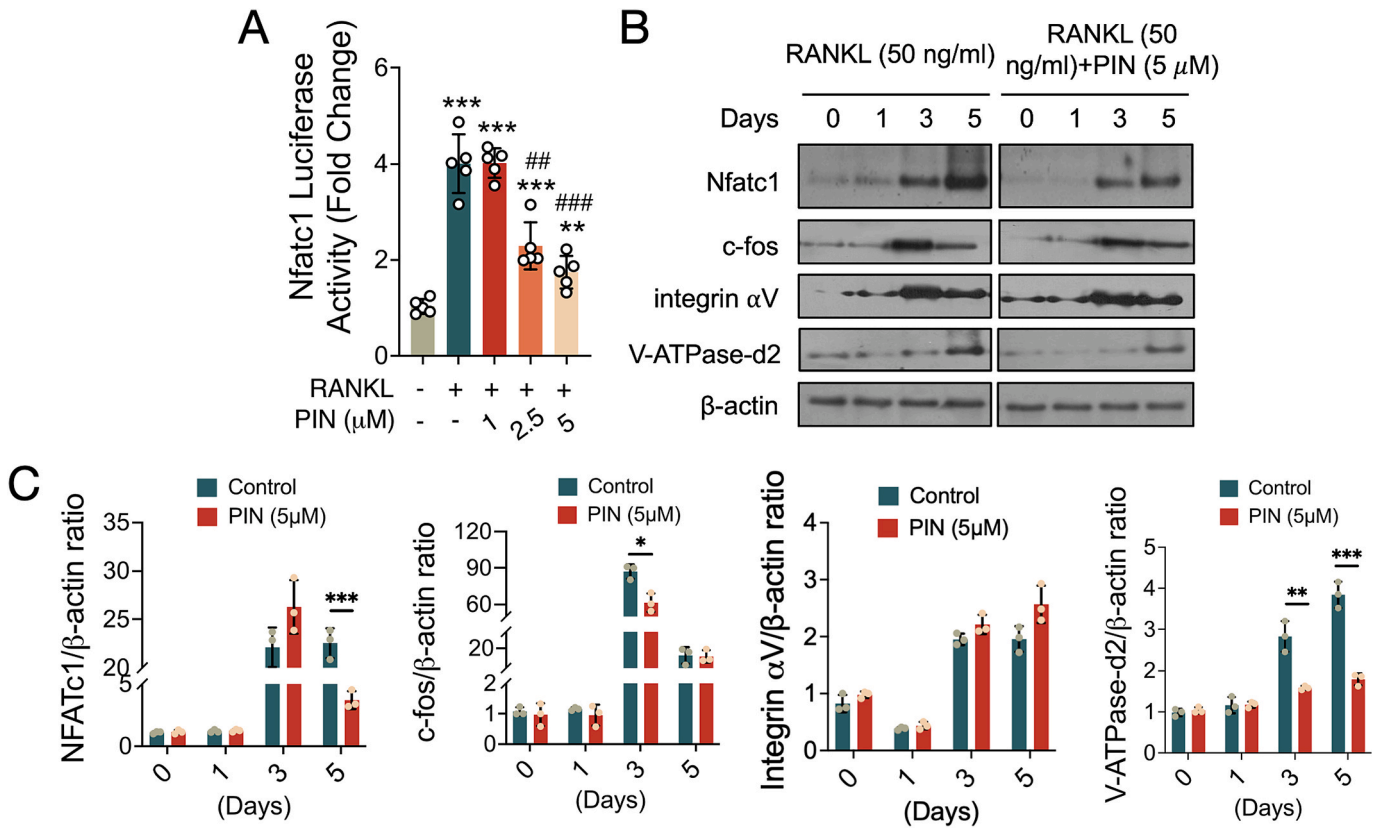

Fig. 6. Impact of PIN on the translocation of Nfatc1 into cell nuclei and its protein expression induced by RANKL. (A) Luciferase gene activity was measured in RAW264.7 cells transfected with Nfatc1 and stimulated with RANKL, using an Nfatc1 luciferase construct. Cells were treated with various doses of PIN and induced with rm-sRANKL (**$P < 0.01$, ***$P < 0.001$, versus blank control. ##$P < 0.01$, ###$P < 0.001$, versus RANKL-treated control). **(B)** Representative images of Western blot analysis using specific antibodies against Nfatc1, c-Fos, integrin αV, V-ATPase-d2, and β-actin. **(C)** The relative protein levels were evaluated by calculating the ratio of Nfatc1, c-Fos, integrin αV and V-ATPase-d2 versus to β-actin. (*$P < 0.05$, **$P < 0.01$, ***$P < 0.01$ compared to RANKL-treated and PIN-untreated controls).

meticulously excised for further assessments. A three-point bending experiment was conducted on the femur of each group of mice, revealing significant improvements in both the yield point (the mechanical force causing absolute damage to the skeleton) and the ultimate force (which indicates the strength of bone) (Fig. 8B). The Micro-CT were truly remarkable: PIN exhibited a profound safeguarding effect against bone loss observed in mice subjected to OVX when compared to the PBS group. This was vividly evident from the notable augmentation in BV/TV and Tb.N, accompanied by a pronounced reduction in trabecular spacing subsequent to PIN administration (Fig. 8C–D). Additionally, in the context of the OVX surgery, PIN effectively reduced both the ratio of osteoclast surface versus bone surface and the ratio of osteoclast number versus bone surface area. This underscores the impressive capacity of PIN to inhibit osteoclast activity in an *in vivo* setting (Fig. 8E–F). Collectively, our findings provide compelling evidence that PIN holds immense promise in counteracting systemic bone loss in ovariectomized animal models.

4. Discussion

It has been well-established that PIN possess the ability to modulate bone homeostasis via regulating osteoblasts and osteocytes [13,14]. In this study, our findings reveal that PIN exerts inhibitory effects on RANKL-induced osteoclastogenesis by effectively reducing both the quantity and dimensions of osteoclasts (see Fig. 9). Additionally, our results demonstrate that PIN significantly suppresses the skeletal resorptive activity of osteoclasts, therefore elucidating the dual impact of PIN on both the initiation and function of osteoclasts.

The development and functioning of osteoclasts are regulated by numerous signaling pathways [15]. Upon RANKL binding to RANK, it activates the bridging protein TRAF6. TRAF6's primary function is to initiate the expression of NFATc1, which is a pivotal transcription factor required for osteoclast formation and the regulation of markers specific to osteoclasts [16–18]. In our current study, we observed that PIN inhibited the movement of NFATc1 triggered by RANKL during the differentiation of osteoclasts in BMMs. The adjustment of NFATc1 activity subsequently influences the expression of genes specific to osteoclasts, including critical ones like *Acp5*, *Cathepsin K*, *Atp6v0d2*, *c-Fos*, and *Mmp9*. These genes, vital for osteoclast formation, were found to be downregulated by PIN [19–22].

Furthermore, RANKL generated reactive oxygen species in mitochondria during electron transport promotes osteoclast growth and differentiation and regulates the degradation of bone matrix [23,24]. According to recent works, RANKL caused induction of downstream signaling (such as NOX1, TRAF6, and Rac1) and diminished the production of anti-oxidant enzymes, thereby augmenting intracellular ROS exposure and osteoclastogenesis [25,26]. To our knowledge, PIN reduced the accumulation of ROS in osteoclasts by inhibiting the expression of TRAF6 and NOX1, which was achieved by lowering the levels of GTP-Rac1 [26,27]. PIN also facilitated the expression of anti-oxidant enzymes, for example, such as HO-1 [28], NADPH-dependent GSR [29], CAT [30]. Thus, of our data suggest that PIN not only restrains ROS accumulation but also enhances ROS scavenging, which naturally then inhibits osteoclast forming and activity.

MAPK are proline-mediated serine/threonine protein kinases, consisting of ERK, p38, and JNK [31]. These factors play crucial roles in intracellular signaling pathways involved in various cellular processes such as growth, development, differentiation, and other physiological

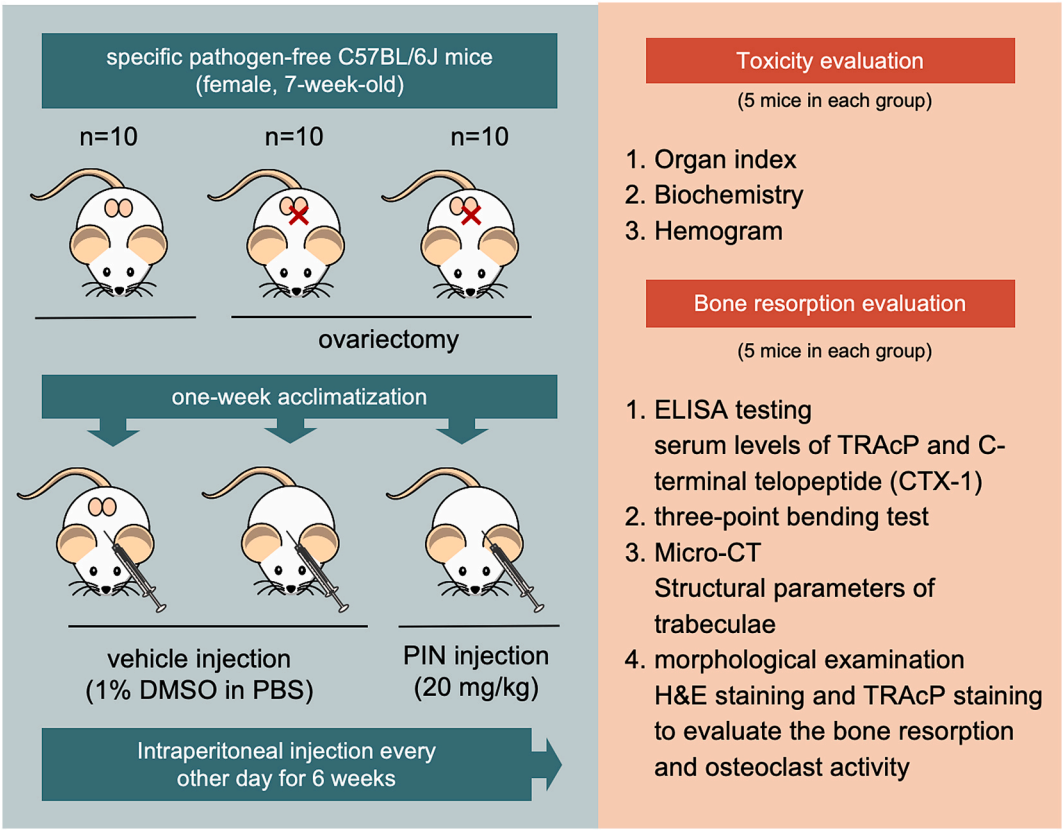

Fig. 7. Illustration of the *in vivo* experimental protocol delineating the assessment of PIN's therapeutic efficacy.

events [32]. Studies have revealed that phosphorylated JNK triggers AP-1 induction, which in turn leads to stimulation of predifferentiation, viability, integration and maturation of osteoclasts [33]. Furthermore, the p38 MAPK pathway is integral to the formation of osteoclasts. Inhibiting the phosphorylation of p38 can have an impact on osteoclastogenesis and the resorption of bone by osteoclasts [34]. c-Fos transcription is mediated by activation of ERK pathway to facilitate osteoclast differentiation [35]. In particular, the ERK pathway promotes the viability of osteoclasts and protects them from the risk of apoptosis [36]. Our study revealed that PIN inhibited the phosphorylation of the above MAPK pathway, implying that PIN represses NFATc1 activity by modulating the MAPK pathway, consequently downmodulating the performance of ATPase-d2 and c-fos functional proteins. The lack of downregulation of Integrin αV by PIN might suggest a selective mechanism of action. Integrin αV is crucial for osteoclast adhesion and the maintenance of the resorption microenvironment [37]. Our findings indicate that while PIN can inhibit certain aspects of osteoclast function, it might not interfere with the adhesion process mediated by Integrin αV. This could have implications for how PIN is integrated into therapeutic strategies, potentially allowing for targeted inhibition of osteoclast activity without compromising cell adhesion and mobility. NF-κB is a crucial transcription factor for osteoclast differentiation [38]. In mice, the disruption of NF-κB signal transduction leads to a failure in osteoclastogenesis and, instead, results in an osteogenic phenotype [39]. In our present study, PIN also poses a significant effect on RANKL-induced NF-κB activity.

Since PIN potently suppresses the forming and function of OCs *in vitro*, an *in vivo* research was performed on a mouse model to identify its effectiveness in preventing OVX-induced femur bone destruction. OVX procedure have previously been shown to cause severe bone destruction in the mouse musculoskeletal system resulting from the estrogen deficiency [40]. Hence, this model can be used to mimic osteoporosis. H&E staining showed distinct bone loss in the carrier group, and TRAP staining displayed a high number of osteoclasts in femur. Following PIN administration, a remarkable reduction in the number of $TRAcP^{+}$ osteoclast-like cells was noted, and OVX-mediated osteolysis was restricted. A possible mechanism for protection of PIN administration from OVX-induced osteolysis may involve suppression of osteoclasts formation and function.

5. Conclusions

Together, these outcomes indicate that PIN may be a potentially effective agent against osteoclast-related osteolysis, yet the broader implications of our findings suggest a potential impact on a range of related diseases. Our investigation into PIN's anti-inflammatory properties indicates promising applications in inflammatory conditions. This insight opens new avenues for research into how PIN could be utilized in the management of inflammatory disorders, including rheumatoid arthritis and Paget's disease. Furthermore, given the antioxidative effects of PIN, its role in diseases where oxidative stress plays a pivotal part warrants further exploration, such as osteonecrosis, osteoarthritis, and fracture nonunion.

However, there are several unresolved issues that emerged from our research. While we have established foundational knowledge about PIN, the translation of these findings into clinical applications remains a significant challenge. Future studies should focus on clinical trials to evaluate the safety and efficacy of PIN in human subjects, particularly in the context of osteolytic conditions. Additionally, the potential synergistic effects of combining PIN with other therapeutic agents represent a promising area for future research. These directions not only address the gaps in our current understanding but also highlight the dynamic and evolving nature of research in this field. Our study serves as a stepping stone towards this goal, contributing valuable insights while also outlining the pathway for future research endeavors.

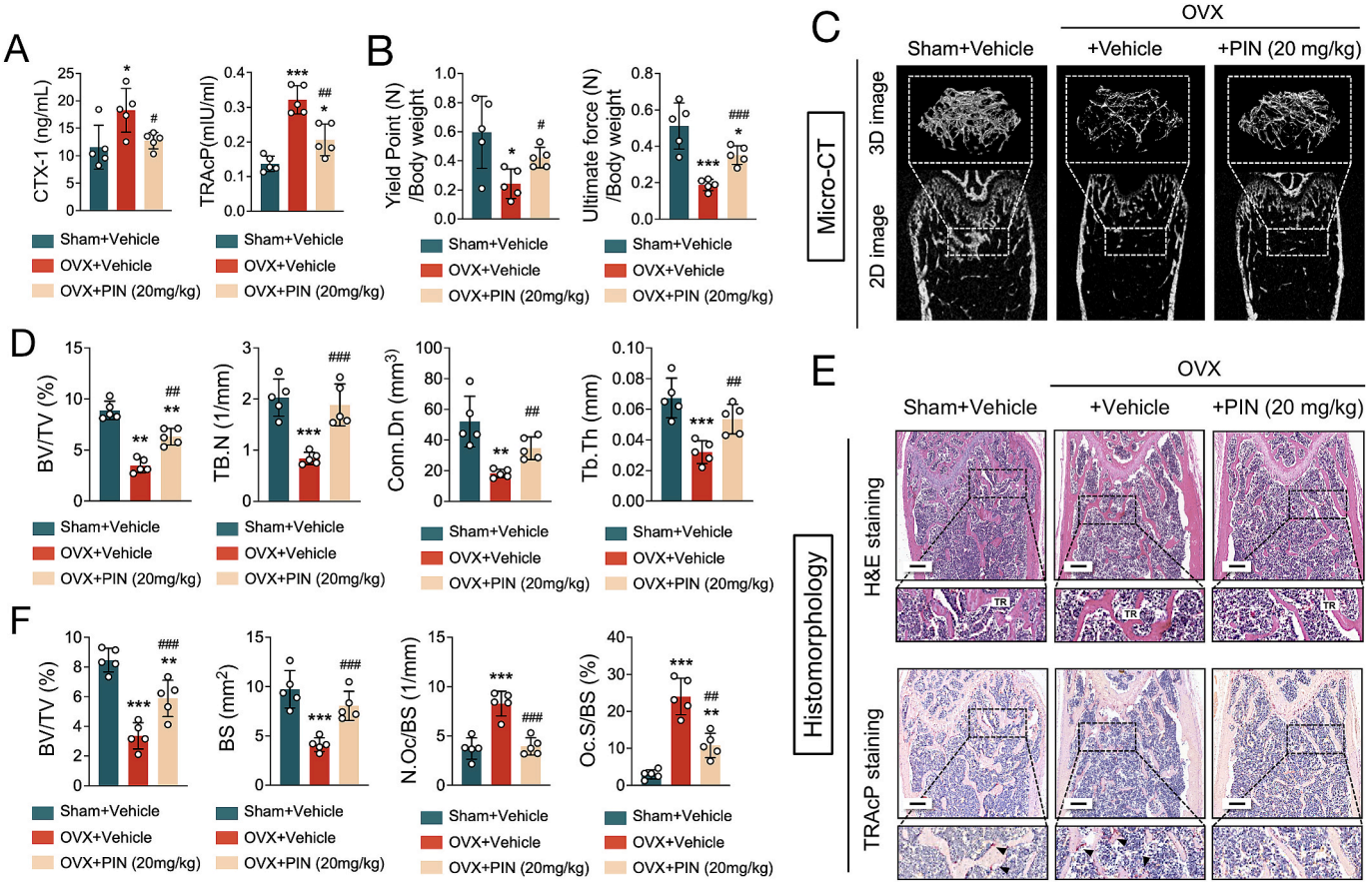

Fig. 8. PIN alleviates bone resorption induced by estrogen deficiency post-ovariectomy, primarily through the suppression of osteoclast activity. (A) This section provides a quantitative assessment of TRAcP and CTX-1 serum concentrations (n = 5). **(B)** Quantitative evaluation of the ultimate force (N) and yield point (N), normalized by body weight, in a group of five mice. **(C)** Representative three-dimensional reconstruction image and micro-CT analysis of trabecular bone microarchitecture. **(D)** Quantitative analysis of BV/TV, Tb.N, Tb.Th, and Tb.Sp for each group (n = 5). **(E)** Representative images of decalcified tissue process by H&E and TRAcP staining. The images are magnified at 4×, with a scale bar of 500 μm. Notably, black arrows point to positive TRAcP staining around trabecula. **(F)** Quantitative analyses of BV/TV, N.Oc/BS, and N.Ob/BS for each group (n = 5). (*P value < 0.05, **P value < 0.01, ***P value < 0.001, versus sham surgery group. #P value < 0.05, ##P value < 0.01, ###P value < 0.001, versus OVX control group).

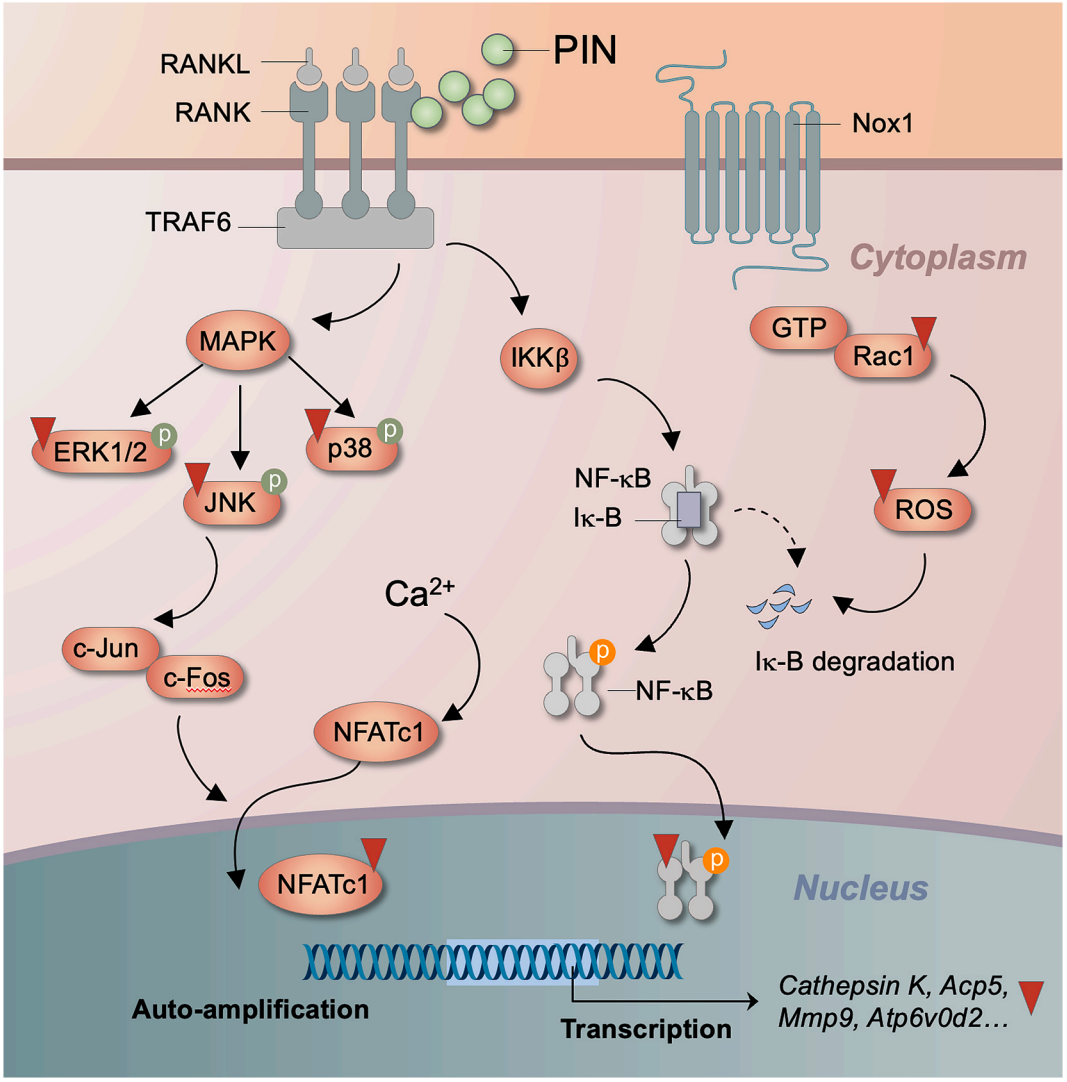

Fig. 9. A schematic illustration outlining the mechanism by which PIN operates during osteoclastogenesis. PIN disrupts the interaction between RANKL and RANK, resulting in the subsequent suppression of both MAPK and NF-κB signaling pathways. Additionally, it influences calcium oscillation. These combined effects culminate in the reduction of NFATc1 nucleus translocation and the production of ROS.

Ethics approval and consent to participate

The animal experimentation was conducted in accordance with the guidelines approved by the Institutional Animal Ethics Committee of Guangzhou University of Chinese Medicine.

Funding

This study was supported in part by the GuangDong Basic and Applied Basic Research Foundation (grant number: 2019A1515110723), China Postdoctoral Science Foundation (grant number: 2023M730809), National Natural Science Foundation of China (grant number: 82305265), and GuangDong Basic and Applied Basic Research Foundation (grant number: 2024A1515010894). The funding body played no role in the design of the study and collection, analysis, and interpretation of data and in writing the manuscript.

Availability of data and materials

The datasets used and/or analysed during the current study are available from the corresponding author on reasonable request.

Authors' contributions

ZC, WH, QW and LZ conceived and supervised the study; GH and SL designed experiments; GH, GZ and QZ performed experiments; QW and LZ provided new tools and reagents; XZ and QZ analysed data; GH wrote the manuscript; WH and ZC made manuscript revisions.

Declaration of competing interest

The authors have declared no conflict of interest.

Abbreviations

PIN	Pinocembrin
NFATc1	nuclear factor of activated T cells 1
MAPK	mitogen-activated protein kinase
OVX	ovariectomized
BMM	bone marrow macrophage
NF-κB	nuclear factor nuclear factor kappa-light-chain-enhancer of activated B cells
RANKL	nuclear factor-κB ligand

ROS	reactive oxygen species
M-CSF	macrophage colony stimulating factor
TRAF6	TNF receptor-associated factor 6
NOX1	nicotinamide adenine dinucleotide phosphate oxidase 1
HO-1	heme oxygenase-1
PFA	paraformaldehyde
c-fos	proto-oncogene C-Fos
Mmp9	matrix metallopeptidase 9
Atp6v0d2	ATPase H+ transporting V0 subunit D2
Acp5	acid phosphatase 5, tartrate resistant
Rac1	Ras-related C3 botulinum toxin substrate 1
CAT	catalase
GTP	guanosine-5′-triphosphate
BV/TV	bone volume per tissue volume
Tb.Th	trabecular thickness
Tb. N	number of trabeculae
Conn.Dn	connectivity density
Oc.S/BS	osteoclast surface/bone surface
N.Oc/BS	number of osteoclasts/bone surface
DCF	dichlorofluorescein
ROI	region of interest

Appendix A. Supplementary data

Supplementary data to this article can be found online at https://doi.org/10.1016/j.jot.2023.12.007.

References

[1] Katsimbri P. The biology of normal bone remodelling. Eur J Cancer Care 2017;26. https://doi.org/10.1111/ecc.12740.

[2] Majidinia M, Sadeghpour A, Yousefi B. The roles of signaling pathways in bone repair and regeneration. J Cell Physiol 2018;233:2937–48. https://doi.org/10.1002/jcp.26042.

[3] Hart NH, Newton RU, Tan J, Rantalainen T, Chivers P, Siafarikas A, et al. Biological basis of bone strength: anatomy, physiology and measurement. J Musculoskelet Neuronal Interact 2020;20:347–71.

[4] Management of osteoporosis in postmenopausal women: the 2021 position statement of the north American menopause society'' editorial panel. Management of osteoporosis in postmenopausal women: the 2021 position statement of the north American menopause society. Menopause News N 2021;28:973–97. https://doi.org/10.1097/GME.0000000000001831.

[5] Kim J-M, Lin C, Stavre Z, Greenblatt MB, Shim J-H. Osteoblast-osteoclast communication and bone homeostasis. Cells 2020;9:E2073. https://doi.org/10.3390/cells9092073.

[6] Reid IR, Billington EO. Drug therapy for osteoporosis in older adults. Lancet Lond Engl 2022;399:1080–92. https://doi.org/10.1016/S0140-6736(21)02646-5.

[7] Kodama J, Kaito T. Osteoclast multinucleation: review of current literature. Int J Mol Sci 2020;21:E5685. https://doi.org/10.3390/ijms21165685.

[8] Udagawa N, Koide M, Nakamura M, Nakamichi Y, Yamashita T, Uehara S, et al. Osteoclast differentiation by RANKL and OPG signaling pathways. J Bone Miner Metabol 2021;39:19–26. https://doi.org/10.1007/s00774-020-01162-6.

[9] Yasuda H. Discovery of the RANKL/RANK/OPG system. J Bone Miner Metabol 2021;39:2–11. https://doi.org/10.1007/s00774-020-01175-1.

[10] Chen X, Wan W, Ran Q, Ye T, Sun Y, Liu Z, et al. Pinocembrin mediates antiarrhythmic effects in rats with isoproterenol-induced cardiac remodeling. Eur J Pharmacol 2022;920:174799. https://doi.org/10.1016/j.ejphar.2022.174799.

[11] Li X, Zhai Y, Xi B, Ma W, Zhang J, Ma X, et al. Pinocembrin ameliorates skin fibrosis via inhibiting TGF-β1 signaling pathway. Biomolecules 2021;11:1240. https://doi.org/10.3390/biom11081240.

[12] Gong L-J, Wang X-Y, Gu W-Y, Wu X. Pinocembrin ameliorates intermittent hypoxia-induced neuroinflammation through BNIP3-dependent mitophagy in a murine model of sleep apnea. J Neuroinflammation 2020;17:337. https://doi.org/10.1186/s12974-020-02014-w.

[13] N N TY, Jt W TT. Effect of pinocembrin isolated from Alpinia zerumbet on osteoblast differentiation. Cytotechnology 2020;73. https://doi.org/10.1007/s10616-020-00427-2.

[14] Wang X-Y, Gong L-J, Huang J-M, Jiang C, Yan Z-Q. Pinocembrin alleviates glucocorticoid-induced apoptosis by activating autophagy via suppressing the PI3K/Akt/mTOR pathway in osteocytes. Eur J Pharmacol 2020;880:173212. https://doi.org/10.1016/j.ejphar.2020.173212.

[15] Ono T, Nakashima T. Recent advances in osteoclast biology. Histochem Cell Biol 2018;149:325–41. https://doi.org/10.1007/s00418-018-1636-2.

[16] Wada T, Nakashima T, Hiroshi N, Penninger JM. RANKL-RANK signaling in osteoclastogenesis and bone disease. Trends Mol Med 2006;12:17–25. https://doi.org/10.1016/j.molmed.2005.11.007.

[17] Park JH, Lee NK, Lee SY. Current understanding of RANK signaling in osteoclast differentiation and maturation. Mol Cell 2017;40:706–13. https://doi.org/10.14348/molcells.2017.0225.

[18] Asagiri M, Takayanagi H. The molecular understanding of osteoclast differentiation. Bone 2007;40:251–64. https://doi.org/10.1016/j.bone.2006.09.023.

[19] Kim K, Lee S-H, Ha Kim J, Choi Y, Kim N. NFATc1 induces osteoclast fusion via up-regulation of Atp6v0d2 and the dendritic cell-specific transmembrane protein (DC-STAMP). Mol Endocrinol Baltim Md 2008;22:176–85. https://doi.org/10.1210/me.2007-0237.

[20] Jacenko O. c-fos and bone loss: a proto-oncogene regulates osteoclast lineage determination. BioEssays News Rev Mol Cell Dev Biol 1995;17:277–81. https://doi.org/10.1002/bies.950170402.

[21] Troen BR. The regulation of cathepsin K gene expression. Ann N Y Acad Sci 2006;1068:165–72. https://doi.org/10.1196/annals.1346.018.

[22] Sundaram K, Nishimura R, Senn J, Youssef RF, London SD, Reddy SV. RANK ligand signaling modulates the matrix metalloproteinase-9 gene expression during osteoclast differentiation. Exp Cell Res 2007;313:168–78. https://doi.org/10.1016/j.yexcr.2006.10.001.

[23] Schieber M, Chandel NS. ROS function in redox signaling and oxidative stress. Curr Biol CB 2014;24:R453–62. https://doi.org/10.1016/j.cub.2014.03.034.

[24] Agidigbi TS, Kim C. Reactive oxygen species in osteoclast differentiation and possible pharmaceutical targets of ROS-mediated osteoclast diseases. Int J Mol Sci 2019;20:3576. https://doi.org/10.3390/ijms20143576.

[25] Tao H, Ge G, Liang X, Zhang W, Sun H, Li M, et al. ROS signaling cascades: dual regulations for osteoclast and osteoblast. Acta Biochim Biophys Sin 2020;52:1055–62. https://doi.org/10.1093/abbs/gmaa098.

[26] Xu Q, Choksi S, Qu J, Jang J, Choe M, Banfi B, et al. NADPH oxidases are essential for macrophage differentiation. J Biol Chem 2016;291:20030–41. https://doi.org/10.1074/jbc.M116.731216.

[27] Lee NK, Choi YG, Baik JY, Han SY, Jeong D-W, Bae YS, et al. A crucial role for reactive oxygen species in RANKL-induced osteoclast differentiation. Blood 2005;106:852–9. https://doi.org/10.1182/blood-2004-09-3662.

[28] Kozakowska M, Szade K, Dulak J, Jozkowicz A. Role of heme oxygenase-1 in postnatal differentiation of stem cells: a possible cross-talk with microRNAs. Antioxidants Redox Signal 2014;20:1827–50. https://doi.org/10.1089/ars.2013.5341.

[29] Aquilano K, Baldelli S, Ciriolo MR. Glutathione: new roles in redox signaling for an old antioxidant. Front Pharmacol 2014;5:196. https://doi.org/10.3389/fphar.2014.00196.

[30] Kanzaki H, Shinohara F, Kanako I, Yamaguchi Y, Fukaya S, Miyamoto Y, et al. Molecular regulatory mechanisms of osteoclastogenesis through cytoprotective enzymes. Redox Biol 2016;8:186–91. https://doi.org/10.1016/j.redox.2016.01.006.

[31] Cargnello M, Roux PP. Activation and function of the MAPKs and their substrates, the MAPK-activated protein kinases. Microbiol Mol Biol Rev MMBR 2011;75:50–83. https://doi.org/10.1128/MMBR.00031-10.

[32] Roux PP, Blenis J. ERK and p38 MAPK-activated protein kinases: a family of protein kinases with diverse biological functions. Microbiol Mol Biol Rev MMBR 2004;68:320–44. https://doi.org/10.1128/MMBR.68.2.320-344.2004.

[33] Lee K, Chung YH, Ahn H, Kim H, Rho J, Jeong D. Selective regulation of MAPK signaling mediates RANKL-dependent osteoclast differentiation. Int J Biol Sci 2016;12:235–45. https://doi.org/10.7150/ijbs.13814.

[34] Thouverey C, Caverzasio J. Focus on the p38 MAPK signaling pathway in bone development and maintenance. BoneKEy Rep 2015;4:711. https://doi.org/10.1038/bonekey.2015.80.

[35] Boyce BF, Yamashita T, Yao Z, Zhang Q, Li F, Xing L. Roles for NF-kappaB and c-Fos in osteoclasts. J Bone Miner Metabol 2005;23(11–5). https://doi.org/10.1007/BF03026317.

[36] Ikeda F, Matsubara T, Tsurukai T, Hata K, Nishimura R, Yoneda T. JNK/c-Jun signaling mediates an anti-apoptotic effect of RANKL in osteoclasts. J Bone Miner Res Off J Am Soc Bone Miner Res 2008;23:907–14. https://doi.org/10.1359/jbmr.080211.

[37] Chin SL, Johnson SA, Quinn J, Mirosavljevic D, Price JT, Dudley AC, et al. A role for alphaV integrin subunit in TGF-beta-stimulated osteoclastogenesis. Biochem Biophys Res Commun 2003;307:1051–8. https://doi.org/10.1016/s0006-291x(03)01294-4.

[38] Boyce BF, Xiu Y, Li J, Xing L, Yao Z. NF-κB-Mediated regulation of osteoclastogenesis. Endocrinol Metab 2015;30:35–44. https://doi.org/10.3803/EnM.2015.30.1.35.

[39] Xu J, Wu HF, Ang ESM, Yip K, Woloszyn M, Zheng MH, et al. NF-kappaB modulators in osteolytic bone diseases. Cytokine Growth Factor Rev 2009;20:7–17. https://doi.org/10.1016/j.cytogfr.2008.11.007.

[40] Lei Z, Xiaoying Z, Xingguo L. Ovariectomy-associated changes in bone mineral density and bone marrow haematopoiesis in rats. Int J Exp Pathol 2009;90:512–9. https://doi.org/10.1111/j.1365-2613.2009.00661.x.